Manipulating the hydrocarbon selectivity of copper nanoparticles in CO2 electroreduction by process conditions

Kas, R.; Kortlever, R.; Yilmaz, H.; Koper, M.T.M.; Mul, G.

ChemPubSoc Europe

DOI: 10.1002/celc.201402373

CHEMELECTROCHEM Communications

Manipulating the Hydrocarbon Selectivity of Copper Nanoparticles in CO_2 Electroreduction by Process Conditions

Recep Kas,[a] Ruud Kortlever,[b] Hasan Yılmaz,[c] Marc T. M. Koper,[b] and Guido Mul*[a]

The formation of ethylene in CO_2 electroreduction over rough copper electrodes is often explained by the presence of specific surface crystal steps, edges and defects. We demonstrate that an identical electrode covered with copper nanoparticles can yield either predominantly ethylene or methane, depending on the electrolyte concentration and applied CO_2 pressure. Calculations of the pH near the electrode surface suggest that ethylene formation is favored by a relatively high (local) pH. Furthermore, the conditions leading to the formation of significant amounts of methane result in rapid deterioration of hydrocarbon production rates, whereas electrode performance in conditions favoring ethylene production can be sustained for hours. This study substantially alters the mechanistic interpretation of formation of ethylene over rough copper surfaces and implies that applied process conditions inducing pH variations near the electrode surface need to be taken into consideration.

Electrochemical CO_2 reduction to CO, formic acid, hydrocarbons and alcohols is currently being extensively investigated, with the aim of achieving an efficient temporary storage of electricity produced by renewable energy sources.[1–3] Many polycrystalline metal electrodes have been analyzed in aqueous, organic, and ionic liquid electrolytes for the conversion of CO_2 to valuable products.[4,5] Electroreduction to CO and formic acid is achieved with high selectivity at low overpotentials in ionic liquids using nanocrystalline metal electrodes, albeit with low current densities.[6,7] Recent theoretical and experimental findings demonstrate that also in aqueous phase electrolytes high CO_2 over proton reduction selectivities can be obtained.[8–12] Copper is a unique electrocatalyst in that hydrocarbons can be produced at ambient pressure.[13] Although long chain hydrocarbons and a variety of products in minor quantities have been reported, the dominant products are methane and ethylene.[14,15] Various studies have demonstrated that the product distribution of electrochemical reduction processes over copper electrodes varies remarkably, depending on the preparation of the copper electrode.[16–18] Recently oxide-derived metal nanoparticles have received a lot of attention due to a higher energy efficiency, selectivity and stability compared to polycrystalline metal electrodes.[18,19] Generally, copper nanoparticles have been reported to show a high faradaic selectivity towards ethylene, as compared to smooth crystalline copper surfaces producing methane.[18] Furthermore, ethane formation was reported by Kanan and co-workers.[19] The selectivity differences observed in various studies discussing copper-induced CO_2 reduction are usually correlated to crystal morphology or roughness of the electrodes, the latter associated with an abundance of specific crystal steps or defects.[18–21] Still, completely different selectivities have been observed on similar morphologies with variation in roughness,[16–18,22] which suggests that the selectivity might have an alternative origin than solely intrinsic catalytic properties. To validate this hypothesis, we studied the effects of electrolyte concentration and CO_2 pressure on the selectivity of methane and ethylene on identical copper nanoparticles in a continuous, pressurized reactor. The selectivity differences experimentally observed are discussed on the basis of the calculated local pH near the electrode surface, and recent (theoretical) findings described in the literature.

Copper nanoparticles on copper substrates were prepared by electrodeposition of cuprous oxide (Cu_2O) from copper lactate solutions and subsequent reduction in 0.1 M $KHCO_3$ (see Figures SI1, SI2, and SI3 in the Supporting Information, SI). The performance of these electrodes was tested at an applied potential of −1.8 V (vs. Ag/AgCl) in a pressurized autoclave under a continuous flow of CO_2, while the gas phase products were analyzed by gas chromatography (GC). The local pH and concentration of species near the electrode surface were calculated using the numerical approach introduced by Gupta et al.[23]

In Figure 1a, the faradaic efficiency (FE) of hydrocarbons at −1.8 V (vs. Ag/AgCl) as a function of electrolyte concentration is shown for similarly prepared electrodes with an initial oxide thickness of 6 μm. The high ethylene over methane ratio (≈30) observed at low electrolyte concentration changes to methane being the dominant product at high electrolyte concentration. The geometrical current density under various conditions is shown in Figure 1b. The high roughness factor of the

[a] R. Kas, Prof. G. Mul
PhotoCatalytic Synthesis Group
MESA+ Institute for Nanotechnology
Faculty of Science and Technology, University of Twente
Meander 229, P.O. Box 217, 7500 AE Enschede (The Netherlands)
E-mail: G.mul@utwente.nl

[b] R. Kortlever, Prof. M. T. M. Koper
Leiden Institute of Chemistry, Leiden University
Einsteinweg 55, P.O. Box 9502
2300 RA Leiden (The Netherlands)

[c] H. Yılmaz
Complex Photonic Systems (COPS)
MESA+ Institute for Nanotechnology
P.O. Box 217, 7500 AE Enschede (The Netherlands)

Supporting Information for this article is available on the WWW under http://dx.doi.org/10.1002/celc.201402373.

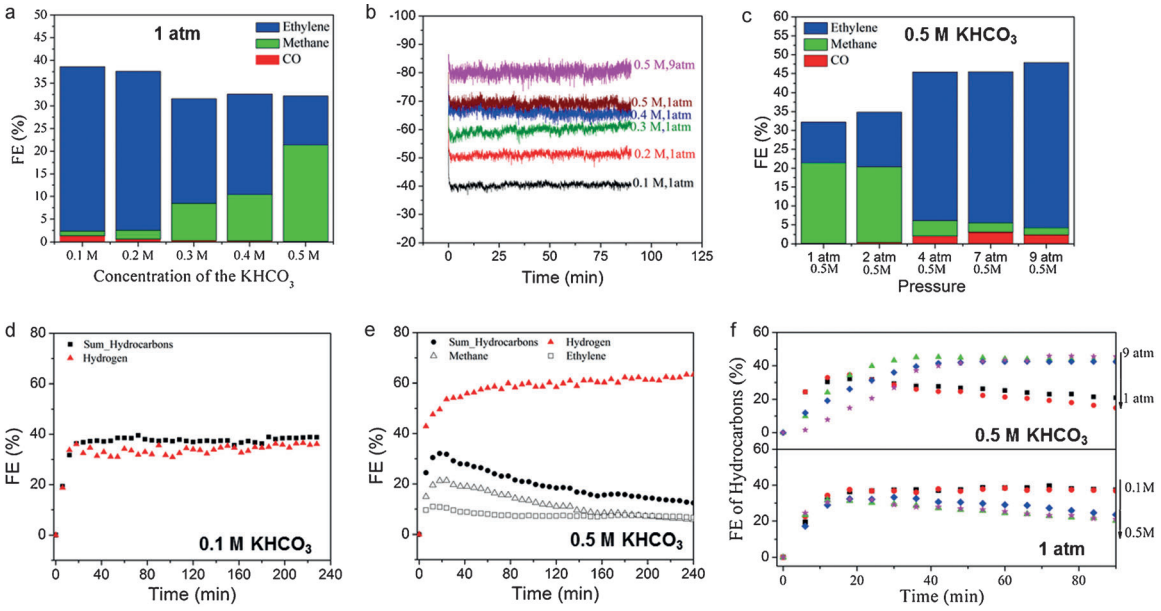

Figure 1. a) Product distributions and b) current densities of CO_2 reduction as a function of electrolyte concentration, and c) as a function of CO_2 pressure. FE of the products versus time graphs are shown in d) 0.1 M $KHCO_3$, 1 atm CO_2 and e) 0.5 M $KHCO_3$ 1 atm CO_2, and f) as a function of pressure and electrolyte concentration (applied potential for all: −1.8 V vs. Ag/AgCl).

electrodes (a roughness factor of ≈16 was determined, Figure SI4), results in the identified high local current densities observed. Figure 1c shows the change in hydrocarbon selectivity as a function of pressure in 0.5 M $KHCO_3$. At 9 atm, the selectivity is comparable to that observed at 1 atm and 0.1 M $KHCO_3$, with FEs of 44% ethylene and 2% methane. In addition, formic acid was detected in the aqueous phase at both low and high pressures of CO_2 (Table SI1). Complete reversibility in selectivity is demonstrated by experiments on one and the same electrode (Figure SI7). Based on the results shown in Figure SI7, any permanent morphological changes that might occur as a result of exposure of the copper surface to high electrolyte concentrations, high currents, and high CO_2 pressures can be excluded.

Figures 1d and 1e show the FE of hydrocarbons and hydrogen versus time at an applied voltage of −1.8 V (vs. Ag/AgCl) in 0.1 M and 0.5 M of $KHCO_3$, respectively. The electrode shows no sign of deactivation over the course of 4 h at 0.1 M of $KHCO_3$, whereas the same electrode producing predominantly methane in 0.5 M $KHCO_3$ deactivates significantly in time with respect to CO_2 reduction efficiency. Hydrogen production is not affected and in fact slowly increases as a function of the reaction time. In Figure 1f, the change in quantity of hydrocarbons is given as a function of time for different electrolyte concentrations (0.1–0.5 M) and pressures (1–9 atm). The time needed to reach steady-state reactor conditions (CSTR approximation) increases as a function of increasing pressure. The deactivation of the electrode at low pressures (1 and 2 atm), when methane is the dominant product, is clearly visible by the continuous decrease in FE at steady-state reactor conditions.

In Figure 2, the calculated pH at the electrode surface is shown as a function of electrolyte concentration for current

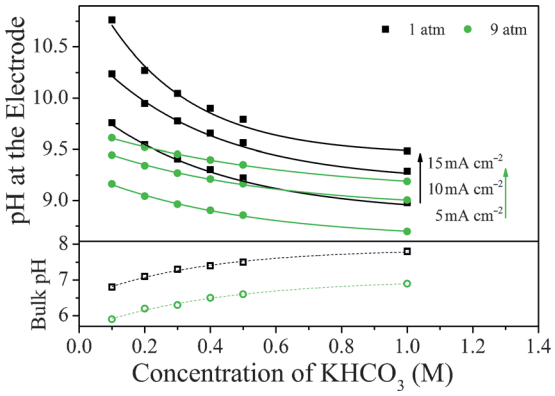

Figure 2. Estimated (local) pH at the electrode surface as a function electrolyte concentration at different current densities and pressures and corresponding bulk pH (independent of current density) for different electrolyte concentrations.

densities of 5, 10 and 15 mA cm^{-2} at 1 and 9 atm. The origin of the high local pH near the electrode surface is the release of OH^- during CO_2 reduction and hydrogen evolution, which increases as a function of increasing current density.[23] An increase in $KHCO_3$ concentration results in an increasing bulk pH and decreasing local pH at the electrode surface, due to the buffer capacity of the electrolyte. An increase in CO_2 concentration induced by high pressures contributes to the buffer capacity of the solution by forming bicarbonate through reaction with OH^-, and consequently, a high CO_2 pressure leads to a lower local pH at similar bicarbonate concentrations (Figure 2). It should be noted that for the calculations, it was assumed that nanoparticles form individual diffusion spheres. The overlap of these diffusion spheres results in the formation of an approximate continuous diffusion layer.[24] So the elec-

trode can be considered as planar, and the diffusion equations can be written accordingly.[25] The only limitation in this approach is that the current densities are evaluated per geometrical area of the electrode, while the electrochemically active surface area is much larger for rough surfaces.

A proposed reaction scheme for electrochemical CO_2 reduction is given in Scheme 1. Hori et al. reported that methane is the dominant product when electropolished polycrystalline copper is used at −1.8 V (vs. Ag/AgCl) in bicarbonate solutions.[26] Concerning the pathway leading to the formation of

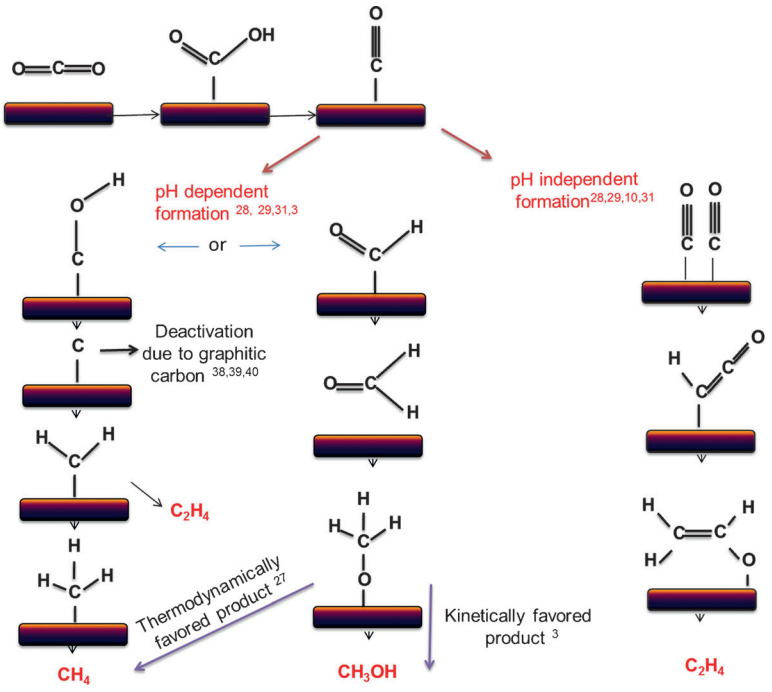

Scheme 1. Reaction scheme for CO_2 reduction.

methane, density functional theory (DFT) calculations on Cu(211) and Cu(100) surfaces indicate that the protonation of CO to CHO on the electrode surface is the rate-determining step for methane formation.[27] This is in agreement with experimental observations that methane formation from CO reduction involves a concerted proton–electron transfer, making its rate pH-dependent on the NHE scale (but pH-independent on the RHE scale).[28–30] Schouten et al. showed that at high potentials, the formation of methane and ethylene from CO occur via a shared intermediate (presumably HCO or COH) on Cu(111) and Cu(100) surfaces, with identical pH dependence.[28,29]

An alternative route to ethylene, a rate-determining CO coupling mechanism, is proposed to take place on Cu(100) surfaces at low overpotential in alkaline media.[8] This step does not include simultaneous proton transfer and is therefore pH-independent on the NHE scale but pH-dependent on the RHE scale, in the sense that the reaction is favored in alkaline media.[10,31] The RHE is the thermodynamically relevant potential scale to compare pH-dependent reactions because it automatically corrects for the pH-dependent equilibrium potential of the overall reaction. As a result, a reaction that involves electron transfer but no proton transfer is pH-dependent on the RHE scale. The formation of ethylene has been found to be especially high in the presence of Cu(100) terrace sites, although there is no clear agreement between long-term electrolysis experiments and shorter-term voltammetry measurements on the optimal (100) terrace width.[32,33]

The identification of two potential pathways for ethylene formation, that is, through a HCO/COH intermediate or CO dimerization, is in agreement with the results of the present study. The formation of ethylene through the CO coupling mechanism is favored at low concentrations of electrolyte due to the correspondingly high local pH near the electrode surface (Figure 2). Such an effect was also emphasized in previous studies where electrolytes with low buffer capacity favor ethylene formation on smooth copper electrodes.[31,34] Increasing the buffer capacity of the solution favors the pathway towards methane, as a result of the lower pH at the electrode surface. The remaining ethylene FE (Figure 1a) might now originate from either the HCO/COH intermediate, or still from CO dimerization.

Higher CO_2 pressures, even though calculated to result in a lower local pH at equal concentration of $KHCO_3$, lead to ethylene most likely because of an increase in local CO concentration and corresponding CO surface coverage. This is also reflected by the increase in the amount of desorbed CO from the surface with increasing pressure (see Figure 1c). In addition, voltammetry studies (Figures 3a and 3b) show a significant reduction peak around −1.1 V (vs. Ag/AgCl) with an onset potential around −0.7 V in linear sweep voltammetry curves in 0.1 and 0.5 M $KHCO_3$ solutions, respectively, specifically at CO_2 pressures larger than 2 atm. On polycrystalline copper, usually no such characteristic peak is observed for CO_2 reduction at 1 atm, and the cathodic current mostly due to hydrogen evolution.[31] Indeed, the peak was not observed at 1 atm, which is consistent with a previous report.[18] The reduction peak emerging at elevated CO_2 pressure is at similar potential as reported for phosphate buffers and high bicarbonate concentrations, in which the CO_2 reduction peak was attributed to bicarbonate reduction and CO adsorption.[35,36]

To gain more insight, long-term product analysis was performed at −1.1 (vs. Ag/AgCl) as a function of increasing pressure (Figure 3c). At high pressures, more time is needed to reach steady-state reactor behavior (CSTR approximation), but

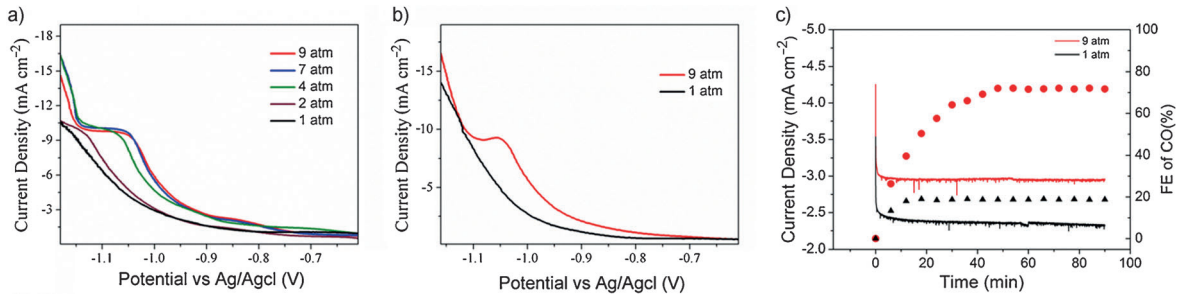

Figure 3. Linear polarization curves for copper nanoparticles in: a) 0.1 M$KHCO_3$ and b) 0.5 M $KHCO_3$ at different pressures and a scan rate of 50 mV s^{-1}. c) Change in current density (line) and FE (scattered) of CO production in 0.1 M $KHCO_3$ at an applied potential of −1.1 V (vs. Ag/AgCl) at 1 and 9 atm.

more importantly, the FE of CO is boosted to 71% at 9 atm compared to 20% at 1 atm under steady-state conditions. The evolution of the reduction peak as a function of pressure follows a very similar trend with the selectivity in CO_2 reduction (see Figure 1c). As the pressure goes up, ethylene formation is favored over methane at −1.8 V (Figure 1c), in agreement with the reduction peak detected at these higher pressures at −1.1 V attributed to the formation of CO (Figure 3b). The rate for C–C coupling at −1.8 V is likely influenced by the surface coverage and local CO concentration in addition to the energetics of the reaction.[15] The high CO selectivity of copper-nanoparticle-containing electrodes at elevated pressures and −1.1 V is thus consistent with the high ethylene selectivity observed at more negative potential (−1.8 V). From a practical point of view, these experiments show that nanoparticle-covered Cu electrodes at moderate CO_2 pressures might be an alternative candidate to Ag, or Au, if a high CO selectivity is desired.

The proposed mechanism for ethylene formation via CO dimerization raises the question why ethylene formation was not observed at low potentials. The onset potential for ethylene formation over nanoparticulate electrodes is around −0.5 V [vs. the reversible hydrogen electrode (RHE)] from CO_2 (Figure SI6), whereas ethylene formation from CO is already observed at −0.2 V (vs. RHE) on Cu(100).[8] This suggests that the first electron transfer, converting CO_2 into CO, is the overall rate-determining step, which involves a concerted proton-coupled electron transfer,[26] whereas the ethylene/methane ratio is determined by the thermodynamic and kinetic barriers associated with the different pathways and the reactant concentrations (protons, dissolved CO) near the electrode surface. In addition, a high local pH may also affect the plots versus the RHE scale, especially at high current densities or potentials. A local pH of 11, for example, would bring an extra electrochemical potential difference of ≈0.25 V with respect to the bulk pH in a 0.1 M $KHCO_3$ solution.

The observation that the deactivation of the electrodes depends on the product made also suggests that methane and ethylene are formed via different pathways. Poisoning has been explained by cathodic deposition of metal impurities during electroreduction by Hori et al.[37] However, due to the very high electrochemically active area of our electrodes, the electrodes are likely not very sensitive to this type of poisoning. In addition to metal deposition, several research groups proposed the deactivation of copper electrodes by graphitic carbon species formed via decomposition of intermediates.[38–40] The product-selective deactivation repetitively observed in the present study suggests that the COH intermediate, relevant in the pH-dependent pathway towards methane on the NHE scale, may be the cause of the deactivation, since the pH-independent CO dimerization mechanism appears to be less sensitive to electrode poisoning.[3,40] There are various previous papers showing that electrodes producing ethylene are stable[16,18,22,41] whereas slow deactivation is reported on roughened electrodes where methane is the major product.[16,39,41]

The fact that the selectivity is governed so sensitively by the process parameters not only clarifies the formation of ethylene on copper nanoparticles in the present study, but likely also the ethylene selectivity observed on roughened copper surfaces prepared ex situ by copper electrodeposition, anodization, pulsed electrolysis, and thermal oxidation.[6,16–18,20–22,39,42,43] On roughened electrodes, the local current density is higher, leading to a very high local pH favoring ethylene formation, while methane production is relatively low. Further increasing the roughness also leads to ethane formation.[19,22] The pathway towards ethane is currently under investigation, but likely related to ethylene hydrogenation.

In summary, we demonstrate that ethylene formation over copper oxide derived copper electrodes can be favored by 1) a low electrolyte concentration and thus buffer capacity, 2) a high local current density (such as on rough electrodes), and 3) high CO_2 pressures. In addition, the experiments show that poisoning species are formed primarily in the methane formation pathway. Local concentrations of reactants (H^+, CO) should be taken into account when mechanistic interpretation of CO_2 reduction results is addressed, in particular in the case of roughened copper surfaces.

Experimental Section

Copper Nanoparticles Preparation

Cuprous oxide films were electrodeposited onto copper plates (Alfa Aesar, 99.99%) from aqueous Cu^{2+}-containing solutions prepared using 0.4 M $CuSO_4$ (Sigma Aldrich, ≥99%) and 4 M lactic acid

(Sigma Aldrich) at 60 °C(1). The pH of the solution was carefully adjusted to pH 12 using solid NaOH pellets (Sigma Aldrich, 98%) and a 1 M NaOH solution. After electrodeposition, the oxide films were reduced back to copper at an applied potential of −1.2 V (vs. Ag/AgCl) in CO_2 saturated 0.1 M $KHCO_3$ (99.99%, Sigma Aldrich). A typical current response to the applied potential is given in Figure SI2. The potential (0.6 V vs. RHE) is enough to reduce Cu_2O back to copper, which starts around 0.3 V (vs. RHE).

Electrochemical CO_2 Reduction

Continuous electrochemical reduction experiments were carried out in a stainless-steel autoclave under continuous stirring at 600 rpm using a magnetic stirrer. The complete operation system is given in Scheme S1 of the SI. Pt mesh was used as the counter electrode and was separated from the working electrode using a proton-exchange Nafion 112 membrane (Sigma Aldrich). Homemade Ag/AgCl in 3 M KCl was used as the reference electrode, which was refreshed and calibrated each week against a reversible hydrogen electrode (RHE). A 50 mL min^{-1} flow rate of CO_2 (Linde Gas Benelux 99.99%) was used before and during the reduction process. The reactor effluent was sampled by GC every 6 min. A thermal conductivity detector (TCD) and flame ionization detector (FID) were used to quantitatively analyze the gas-phase products. The time needed to reach the steady-state concentration varied within the range of 25–45 min depending on the pressure, so all experiments were conducted for at least 90 min (see the SI for further details).

Acknowledgements

This work was supported by NanoNextNL, a micro and nanotechnology consortium of the Government of the Netherlands and 130 partners. We would like to thank FOM for support and Sander Koper for the liquid chromatography measurements.

Keywords: carbon monoxide · electrochemical CO_2 reduction · local pH · pressure · selectivity

[1] B. Kumar, M. Asadi, D. Pisasale, S. Sinha-Ray, B. A. Rosen, R. Haasch, J. Abiade, A. L. Yarin, A. Salehi-Khojin, *Nat. Commun.* **2013**, *4*, 2819.
[2] J. L. DiMeglio, J. Rosenthal, *J. Am. Chem. Soc.* **2013**, *135*, 8798 – 8801.
[3] X. Nie, M. R. Esopi, M. J. Janik, A. Asthagiri, *Angew. Chem. Int. Ed.* **2013**, *52*, 2459 – 2462; *Angew. Chem.* **2013**, *125*, 2519 – 2522.
[4] E. V. Kondratenko, G. Mul, J. Baltrusaitis, G. O. Larrazábal, J. Pérez-Ramírez, *Energy Environ. Sci.* **2013**, *6*, 3112 – 3135.
[5] D. T. Whipple, P. J. Kenis, *J. Phys. Chem. Lett.* **2010**, *1*, 3451 – 458.
[6] S. Zhang, P. Kang, T. J. Meyer, *J. Am. Chem. Soc.* **2014**, *136*, 1734 – 1737.
[7] B. A. Rosen, A. Salehi-Khojin, M. R. Thorson, W. Zhu, D. T. Whipple, P. J. Kenis, R. I. Masel, *Science* **2011**, *334*, 643 – 644.
[8] K. J. P. Schouten, Z. Qin, E. P. r. Gallent, M. T. M. Koper, *J. Am. Chem. Soc.* **2012**, *134*, 9864 – 9867.
[9] C. W. Li, J. Ciston, M. W. Kanan, *Nature* **2014**, *508*, 504 – 507.
[10] F. Calle-Vallejo, M. T. M. Koper, *Angew. Chem. Int. Ed.* **2013**, *52*, 7282 – 7285; *Angew. Chem.* **2013**, *125*, 7423 – 7426.
[11] J. H. Montoya, A. A. Peterson, J. K. Nørskov, *ChemCatChem* **2013**, *5*, 737 – 742.
[12] K. J. P. Schouten, F. Calle-Vallejo, M. T. M. Koper, *Angew. Chem. Int. Ed.* **2014**, *53*, 10858 – 10860; *Angew. Chem.* **2014**, *126*, 11036 – 11038.
[13] Y. Hori, K. Kikuchi, S. Suzuki, *Chem. Lett.* **1985**, 1695 – 1698.
[14] H. Shibata, J. A. Moulijn, G. Mul, *Catal. Lett.* **2008**, *123*, 186 – 192.
[15] K. P. Kuhl, E. R. Cave, D. N. Abram, T. F. Jaramillo, *Energy Environ. Sci.* **2012**, *5*, 7050 – 7059.
[16] M. R. Gonçalves, A. Gomes, J. Condeco, R. Fernandes, T. Pardal, C. Sequeira, J. Branco, *Energy Convers. Manage.* **2010**, *51*, 30 – 32.
[17] M. R. Gonçalves, A. Gomes, J. Condeço, T. Fernandes, T. Pardal, C. Sequeira, J. Branco, *Electrochim. Acta* **2013**, *102*, 388 – 392.
[18] W. Tang, A. A. Peterson, A. S. Varela, Z. P. Jovanov, L. Bech, W. J. Durand, S. Dahl, J. K. Nørskov, I. Chorkendorff, *Phys. Chem. Chem. Phys.* **2012**, *14*, 76 – 81.
[19] C. W. Li, M. W. Kanan, *J. Am. Chem. Soc.* **2012**, *134*, 7231 – 7234.
[20] S. Sen, D. Liu, G. T. R. Palmore, *ACS Catal.* **2014**, *4*, 3091 – 3095.
[21] O. Baturina, Q. Lu, M. Padilla, L. Xin, W. Li, A. Serov, P. Atanassov, F. Xu, A. Epshteyn, T. H. Brintlinger, *ACS Catal.* **2014**, *4*, 3682 – 3695.
[22] R. Kas, R. Kortlever, A. Milbrat, M. T. M. Koper, G. Mul, J. Baltrusaitis, *Phys. Chem. Chem. Phys.* **2014**, *16*, 12194 – 12201.
[23] N. Gupta, M. Gattrell, B. MacDougall, *J. Appl. Electrochem.* **2006**, *36*, 161 – 172.
[24] B. Wickman, Y. E. Seidel, Z. Jusys, B. Kasemo, R. J. Behm, *ACS Nano* **2011**, *5*, 2547 – 2558.
[25] S. E. Kleijn, S. Lai, M. T. M. Koper, P. R. Unwin, *Angew. Chem. Int. Ed.* **2014**, *53*, 3558 – 3586.
[26] Y. Hori, *Mod. Aspects Electrochem.* **2008**, *42*, 89 – 189.
[27] A. A. Peterson, F. Abild-Pedersen, F. Studt, J. Rossmeisl, J. K. Nørskov, *Energy Environ. Sci.* **2010**, *3*, 1311 – 1315.
[28] K. J. P. Schouten, E. Pérez Gallent, M. T. M. Koper, *J. Electroanal. Chem.* **2014**, *716*, 53 – 57.
[29] Y. Hori, R. Takahashi, Y. Yoshinami, A. Murata, *J. Phys. Chem. B* **1997**, *101*, 7075 – 7081.
[30] M. T. M. Koper, *Chem. Sci.* **2013**, *4*, 2710 – 2723.
[31] M. Gattrell, N. Gupta, A. Co, *J. Electroanal. Chem.* **2006**, *594*, 1 – 19.
[32] Y. Hori, I. Takahashi, O. Koga, N. Hoshi, *J. Mol. Catal. A* **2003**, *199*, 39 – 47.
[33] K. J. P. Schouten, E. Pérez Gallent, M. T. M. Koper, *ACS Catal.* **2013**, *3*, 1292 – 1295.
[34] Y. Hori, A. Murata, R. Takahashi, *J. Chem. Soc. Faraday Trans. 1* **1989**, *85*, 2309 – 2326.
[35] R. Kortlever, K. Tan, Y. Kwon, M. T. M. Koper, *J. Solid State Electrochem.* **2013**, *17*, 1843 – 1849.
[36] Y. Hori, A. Murata, R. Takahashi, S. Suzuki, *J. Chem. Soc. Chem. Commun.* **1988**, 17 – 19.
[37] Y. Hori, H. Konishi, T. Futamura, A. Murata, O. Koga, H. Sakurai, K. Oguma, *Electrochim. Acta* **2005**, *50*, 5354 – 5369.
[38] D. W. DeWulf, T. Jin, A. J. Bard, *J. Electrochem. Soc.* **1989**, *136*, 1686 – 1691.
[39] G. Kyriacou, A. Anagnostopoulos, *J. Electroanal. Chem.* **1992**, *322*, 233 – 246.
[40] J.-F. Xie, Y.-X. Huang, W.-W. Li, X.-N. Song, L. Xiong, H.-Q. Yu, *Electrochim. Acta* **2014**, *139*, 137 – 144.
[41] C. S. Chen, A. D. Handoko, J. H. Wan, L. Ma, D. Ren, B. S. Yeo, *Catal. Sci. Technol.* **2015**, DOI: 10.1039/C4CY00906A.
[42] J. Bugayong, G. L. Griffin, *ECS Trans.* **2013**, *58*, 81 – 89.
[43] G. L. Griffin, J. Bugayong, *MRS Online Proc. Libr.* **2014**, *1677*, 2014.

Received: November 5, 2014
Published online on December 9, 2014